Int. J. Electrochem. Sci., 8 **(2013)** 4551 - 4559

International Journal of
ELECTROCHEMICAL
SCIENCE
www.electrochemsci.org

Synthesis and Characterization of $CaTi_2O_4(OH)_2$ Nanosheets for Lithium-Ion Battery

Weixia Dong[1,2], *Bin Song*[3,*], *Gaoling Zhao*[1] *and Gaorong Han* [1]

[1] State Key Laboratory of Silicon Materials & Department of Materials Science and Engineering, Zhejiang University, Hangzhou, 310027, P. R. China
[2] Department of material Science and Engineering, Jingdezhen Ceramic Institute, Jingdezhen, 333001, P. R. China
[3] Department of Physics, Zhejiang University, Hangzhou, 310027, P. R. China
[*]E-mail: bzsong@css.zju.edu.cn

Received: 11 January 2013 / *Accepted:* 25 February 2013 / *Published:* 1 April 2013

Pure and lithium ion doped $CaTi_2O_4(OH)_2$ nanosheets were prepared by a hydrothermal method without template or surfactant. X-ray diffraction (XRD), Brunauer-Emmett-Teller (BET), field emission scanning electron microscopy (FESEM) and transmission electron microscopy (TEM) were carried out to investigate the microstructure of the samples. The results showed that the samples own mesoporous structure. Introducing lithium ion improved the surface area and crystal lattice constant of $CaTi_2O_4(OH)_2$, but decreased the crystal size. Moreover, the electrochemical properties of $CaTi_2O_4(OH)_2$ nanosheets for lithium-ion batteries were improved by introducing lithium ion.

Keywords: $CaTi_2O_4(OH)_2$ nanosheets; lithium ion; cyclability

1. INTRODUCTION

Layered metal hydroxides (LDHs) are a class of important lamellar materials. [1-3] They are described by the general formula $[M^{II}_{(1-x)}M^{III}_x(OH)_2]^{x+}[A^{m-}]_{x/m}\cdot nH_2O$, where M_{II} and M_{III} represent metallic cations and A^{m-} the interlayer anion. The layered structure of the double-layered hydroxide is constructed by the periodic stacking of positively charged (M^{II}, M^{III}) $(OH)_2$ octahedral layers related to brucite, balanced by interlayer anions and water molecules that bind the sheets together. The layered-structure materials give rise to a range of applications including catalysts and catalyst precursors, adsorbers, capacitors and stabilizers, etc. [4-9] $CaTi_2O_4(OH)_2$, which is usually obtained during the preparation of $CaTiO_3$, is a layered metal hydroxide material. It should have similar properties with LDHs. Considering layered and open-framework crystal structure, it is highly prospective in terms of reversible incorporation of lithium ions, and makes its use in the lithium-ion batteries possible.

Recently, our studies found that $CaTi_2O_4(OH)_2$ nanosheets exhibit certain electrochemical properties. In particular, $CaTi_2O_4(OH)_2$ nanosheets by introducing lithium ions could significantly improve the performance of lithium cells. To our knowledge, the preparation and properties of stable $CaTi_2O_4(OH)_2$ have not been reported. Therefore, it is a challenging research to explore its properties by a simple method.

In this paper, we report the synthesis of $CaTi_2O_4(OH)_2$ by a hydrothermal process without template or surfactant. Effects of amount of lithium ion (x) on the electrochemical properties of $CaTi_2O_4(OH)_2$ for lithium-ion batteries have been discussed.

2. EXPERIMENTAL

2.1. Synthesis of the samples

Titanium n-butoxide (TBOT), lithium chloride ($LiCl{\cdot}H_2O$) and calcium chloride ($CaCl_2$) were used as the precursor. The composition of the starting materials was $CaCl_2$: TBOT: water: ethanol molar ratio =1: 1: 400: 10. TBOT ethanol solution was added to $CaCl_2$ and $LiCl{\cdot}H_2O$ mixed aqueous solution (the Li: Ca molar ratio x was kept as 0, 0.05, 0.2, 0.4, 0.6 and 0.8, respectively) in Teflon-lined steel autoclaves, forming suspension A. After suspension A was stirred for 10 min, 3 M KOH was added to suspension A to adjust the pH value to 8~8.2, the mixing suspension was always performed under vigorous stirring at room temperature. Subsequently, the autoclave was sealed, and heated up to 180 ^oC for 36 h, followed by a natural cooling to room temperature. The white powders were collected, thoroughly washed and dried at 80 ^oC for 12 h under a vacuum oven. The samples with various lithium ion content are obtained, hereafter named as $Li_xCaTi_2O_4(OH)_2$ (x= 0, 0.05, 0.2, 0.4, 0.6 and 0.8).

2.2. Characterization of the samples

The crystal phases of the samples were characterized by X-ray diffraction (XRD, PANalytical X'Pert Pro, Holland), in a 2θ range from 5^o to 80^o, using Cu-Ka radiation (λ =0.15420 nm) operating at 50 kV and 40 mA. The morphologies and microstructure of the samples were characterized by a field emission scanning electron microscopy (FESEM, Hitachi S-4800, Japan) operating at an accelerating voltage of 5.0 kV, and transmission electron microscopy (TEM) operating at an accelerating voltage of 160 KV. Nitrogen adsorption–desorption isotherms were collected at 77 K using a Micromeritics TriStar ii 3020 analyzer.

2.3. Electrochemical measurement of the samples

Electrochemical experiments were carried out by assembling coin-type model cells using lithium foil as the counter and reference electrode. The working electrode for the model cells was fabricated by compressing a mixture of 85 wt% $Li_xCaTi_2O_4(OH)_2$ sample, 10 wt% acetylene black,

and 5 wt% poly (tetrafluoroethylene) onto an aluminium foil. The electrolyte was 1 M $LiPF_6$ (Merck, battery grade) in a mixture of ethyl carbonate (EC) and diethyl carbonate (DMC) (1:1 in vol. ratio). Coin-type cells were assembled in a glove-box filled with pure argon. The charge–discharge measurement was carried out at a 0.1 mA cm^{-2} (0.1 C rate) at room temperature using a Neware battery test system BTS-XWJ-6.83S-2010320 (Newell, Shenzhen, China).

3. RESULTS AND DISCUSSION

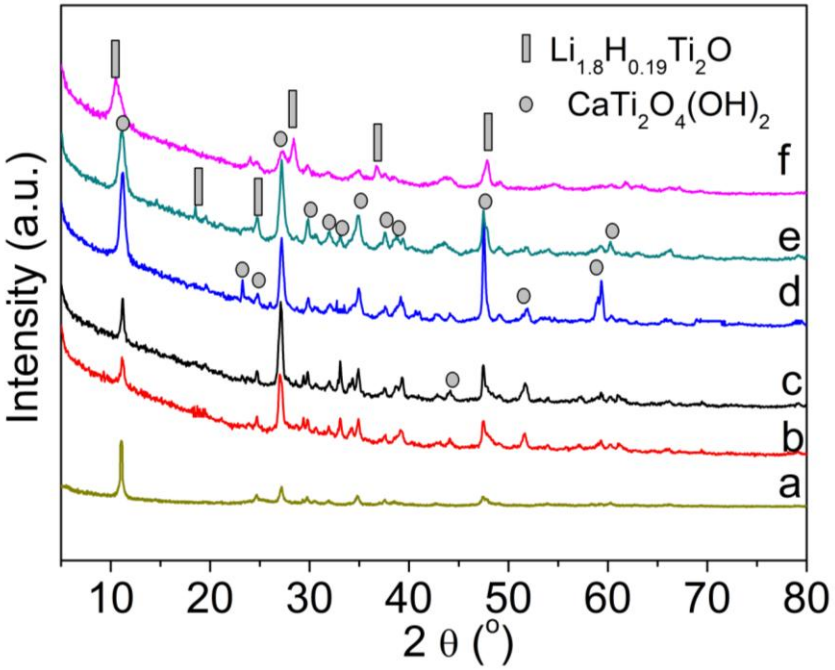

Figure 1. XRD patterns of $Li_xCaTi_2O_4(OH)_2$ samples with various x: (a) 0 , (b) 0.05 , (c) 0.2 , (d) 0.4 , (e) 0.6 , (f) 0.8 .

Fig. 1 shows XRD pattern of $Li_xCaTi_2O_4(OH)_2$ samples with various x. When x is equal or lesser than 0.4, all diffraction peaks can be well indexed to $CaTi_2O_4(OH)_2$ (JCPDS card 39-0357).The crystallinity (X) of each sample is calculated from XRD data by using the following equation: $X=\frac{I_d}{I_t}\times 100\%$, where I_d is intensity of the crystalline diffraction peaks, and I_t is sum of the intensities of the sample. [10] The average crystalline size of $Li_xCaTi_2O_4(OH)_2$ samples is calculated by Scherrer formula: $d=\frac{k\lambda}{\beta\cos\theta}$, where d is the average crystallite size, k is 0.9, λ is the wavelength of Cu Kα (i.e. λ =0.15420 nm), β is the full width at half maximum intensity of the peak (FWHM) in radian and θ is Bragg's diffraction angle. [10] The lattice parameters and cell volume are calculated by Fourier synthesis with the program SHELXS−97. [11] The crystallinity, average crystalline size and lattice parameters a, c are summarized in Table 1. As shown in Table 1, the crystallinity of the samples is around 79%, and doesn't change obviously with x. The crystalline size decreases with the increase of

x. The lattice parameter a is almost same values with the increase of x. But the values of the lattice parameter c and cell volume increase with the increase of x. As for hydrotalcite-type structure, the lattice parameter a corresponds to the average cation-cation distance in the brucite-like layers, and c is related to the total thickness of the brucite-like layer and the interlayer distance. [12-13] According to the increasing c value with x (Table 1), it can be suggested that lithium ions insert the interlayer of $CaTi_2O_4(OH)_2$. When x is 0.6 or more, $Li_{1.8}H_{0.19}Ti_2O$ phase appears in the samples.

Table 1. the crystallinity, crystalline size and lattice parameters of $Li_xCaTi_2O_4(OH)_2$ samples with various x

x (mol)	Crystallinity (%), X	Crystalline size (nm)	Lattice patameter/ Å		Cell volume Å^3
			a	c	
0	79.93	50.1	12.09277	4.94456	1894.49
0.05	79.71	45.5	12.09280	4.94857	1894.92
0.2	79.62	19.0	12.09253	4.95629	1897.08
0.4	79.38	15.4	12.09297	4.95939	1897.20

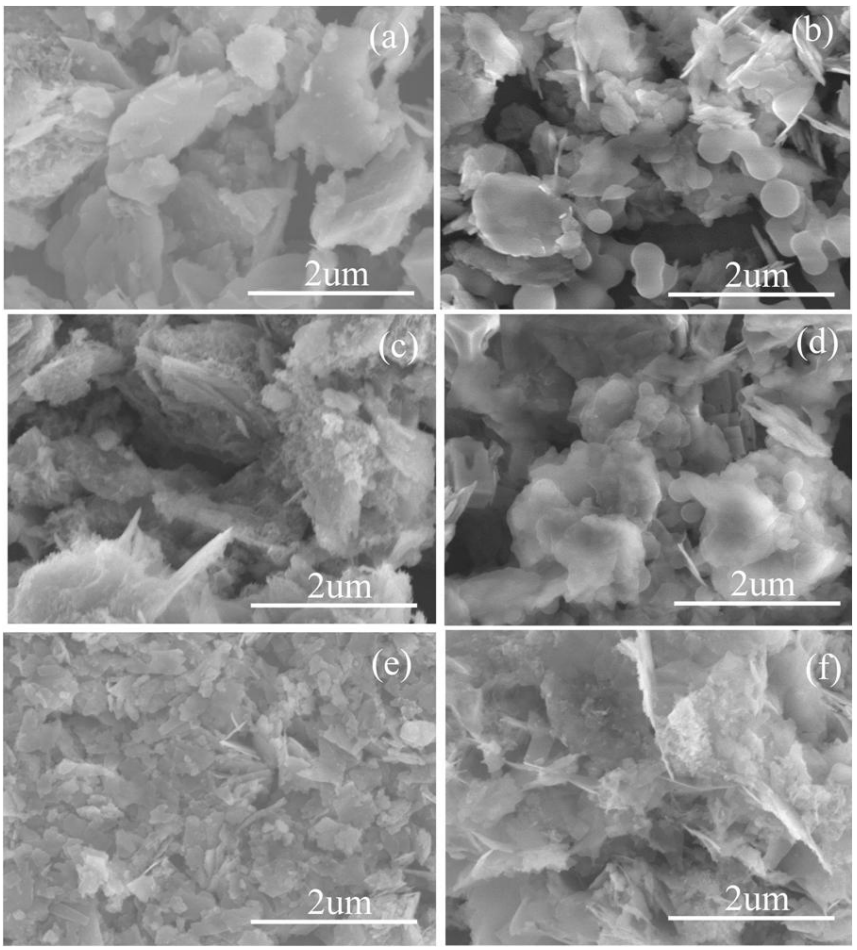

Figure 2. FESEM images of $Li_xCaTi_2O_4(OH)_2$ samples with various x: (a) 0 , (b) 0.05 , (c) 0.2 , (d) 0.4 , (e) 0.6 , (f) 0.8.

Fig. 2 shows SEM images of $Li_xCaTi_2O_4(OH)_2$ samples with various x. When x is equal or lesser than 0.4, Fig. 2(a)-(d) exhibit similarly agglomerated stacking sheet-like morphology. The average particle size of nanosheets is about hundreds of nanometers. When x is 0.6 or more, Fig. 2(e)-(f) show the dense nanosheet-like morphology.

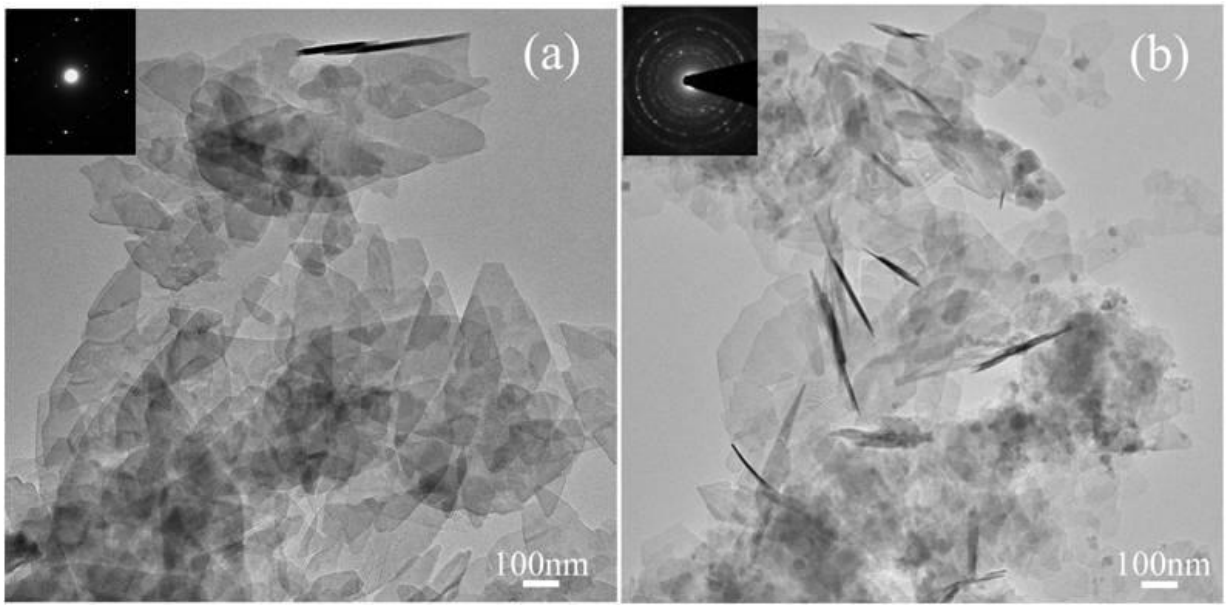

Figure 3. TEM images and the corresponding SAED pattern (inset) of $Li_xCaTi_2O_4(OH)_2$ samples with various x : (a) 0 , (b) 0. 4 .

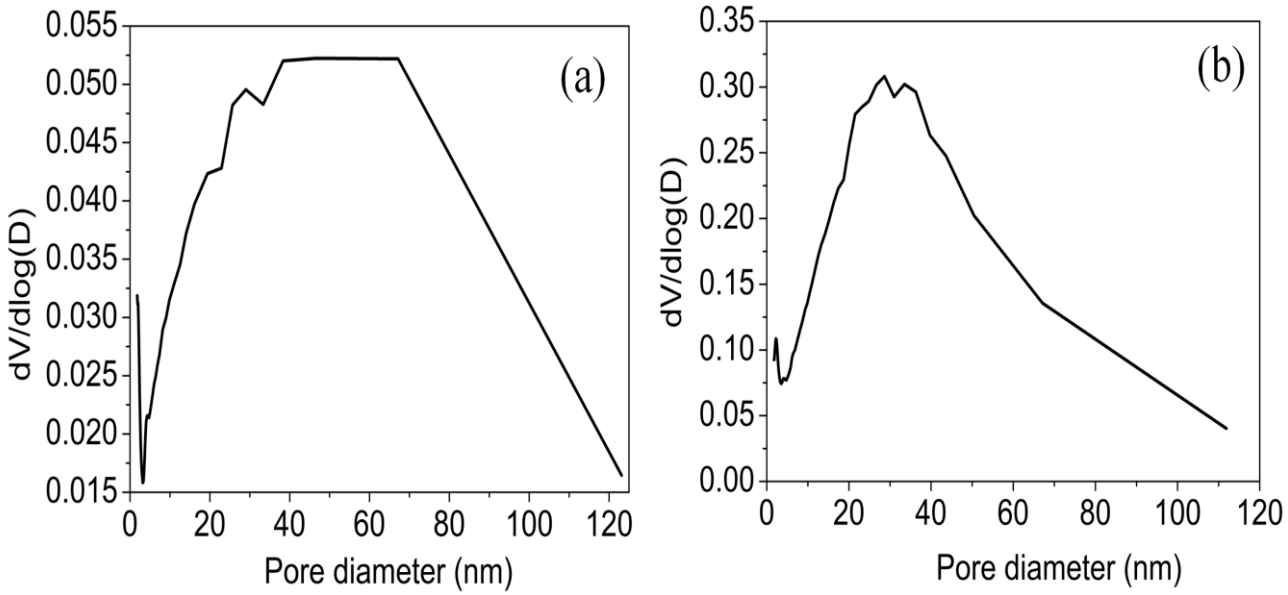

Figure 4. BJH-adsorption pore size distributions of $Li_xCaTi_2O_4(OH)_2$ samples with various x : (a) 0, (b) 0. 4.

Fig. 3 shows TEM images and the corresponding selected area electron diffraction (SAED) pattern of $Li_xCaTi_2O_4(OH)_2$ samples with x=0 and 0.4, respectively. Fig. 3(a) shows the sample consists of lots of the stacking nanosheets. Inset of Fig. 3(a) is the electron diffraction spots of $CaTi_2O_4(OH)_2$ sample, showing a single crystalline structure. Fig. 3(b) shows the TEM image of $Li_{0.4}CaTi_2O_4(OH)_2$ sample. Most of the sample maintains nanosheet-like morphology and some nanoparticles coexist. Inset of Fig. 3(b) shows that the SAED pattern of $Li_{0.4}CaTi_2O_4(OH)_2$ sample, indicating a polycrystalline structure.

Fig. 4 shows the Barrett-Joyner-Halenda (BJH) pore size distribution plots of $CaTi_2O_4(OH)_2$ and $Li_{0.4}CaTi_2O_4(OH)_2$ samples, respectively. The BET surface areas of $Li_{0.4}CaTi_2O_4(OH)_2$ and $CaTi_2O_4(OH)_2$ samples are 93.0 and 25.8 m^2/g, respectively. The BET surface area of $Li_{0.4}CaTi_2O_4(OH)_2$ sample is increased by more than three times compared with that of $CaTi_2O_4(OH)_2$ sample. This can be ascribed to the smaller size than that of $CaTi_2O_4(OH)_2$ sample (See Table 1). The BJH average pore diameter calculated from the adsorption branch of the isotherms are 10.9 nm and 10.7 nm for $Li_{0.4}CaTi_2O_4(OH)_2$ and $CaTi_2O_4(OH)_2$ samples, respectively. The mesoporous structure can be attributed to the porous stacking of nanosheets. [15-16]

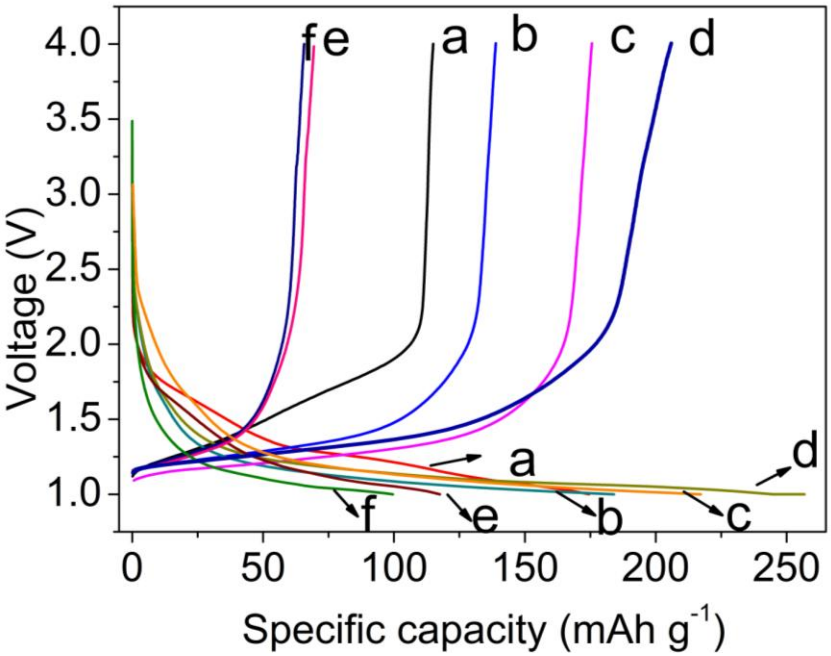

Figure 5. First cycle charge/discharge curves of $Li_xCaTi_2O_4(OH)_2$ samples with various x: (a) 0 , (b) 0.05 , (c) 0.2 , (d) 0.4 , (e) 0.6 , (f) 0.8.

Fig. 5 shows the initial cycle charge/discharge curves of $Li_xCaTi_2O_4(OH)_2$ (x= 0, 0.05, 0.2, 0.4, 0.6 and 0.8) samples at 0.1 C. When x is 0, 0.05, 0.2, 0.4, 0.6 and 0.8, $Li_xCaTi_2O_4(OH)_2$ nanosheets exhibit an initial discharge capacity of 174.4, 184.1, 206, 256.8, 117.5 and 99.6 mAh/g, respectively. When x is equal or lesser than 0.4, the discharge capacity increases with x and reaches an optimum at x=0.4. Further increasing x ($\geq$ 0.6 mol) decreases the discharge capacity.

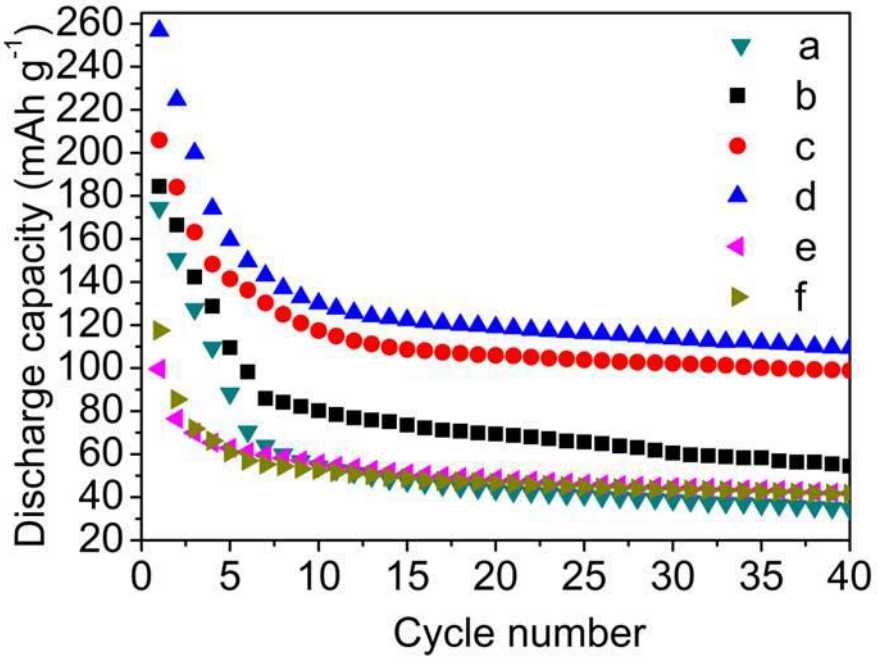

Figure 6. Cycling performance of $Li_xCaTi_2O_4(OH)_2$ samples with various x: (a) 0 , (b) 0.05 , (c) 0.2 , (d) 0.4 , (e) 0.6 , (f) 0.8.

Fig. 6 shows $Li_xCaTi_2O_4(OH)_2$ (x=0, 0.05, 0.2, 0.4, 0.6 and 0.8) samples possess comparable cycling performance between 1.0 and 4.0 V under a constant current densities of 1mA/g up to 40 cycles at 0.1 C. Despite of the relatively faster capacity fading behavior, $Li_{0.4}CaTi_2O_4(OH)_2$ sample always possesses higher capacity compared with the pristine $CaTi_2O_4(OH)_2$. Moreover, compared with irreversible loss of 33.2% of pristine $CaTi_2O_4(OH)_2$, $Li_{0.4}CaTi_2O_4(OH)_2$ sample exhibits the lower initial irreversible loss of 11.4%. A large drop in capacity is obviously seen in Fig. 6 for all the samples because of the initial irreversible loss. From the 5th to 40 th, the discharge capacity of $Li_{0.4}CaTi_2O_4(OH)_2$ keeps a steady level from 149.6 to 128.2 mAh/g, and the rate efficiency achieves as high as 86%. However, the rate efficiency of $CaTi_2O_4(OH)_2$ is 67%. After 40 cycles, $Li_{0.4}CaTi_2O_4(OH)_2$ sample shows an improved cyclic durability, which is higher than that of pure $CaTi_2O_4(OH)_2$ sample.

The effects of the amount of lithium ion (x) on the electrochemical properties can be ascribed to the lattice parameters, crystal size and specific surface areas of the samples. Firstly, it is known that the expansion in crystal lattice could provide more space for lithium intercalation/de-intercalation and relieve the stress caused by severe volume change during the cycle process. The nanosheet-like morphology and the small size of the particles are favorable for the intercalation/de-intercalation process. [16-17] When x is equal or lesser than 0.4, the lattice parameter c slightly increase with x (Table 1), resulting in more space for lithium intercalation/de-intercalation. Thus the electrochemical properties increase with x. Secondly, the average size of the crystal decreases with the increase of x (Table 1), which could shorten the diffusion length of lithium ion, and improves the lithium ion and electronic conduction, therefore, the specific capacity improve with the increase of x. Thirdly, high specific surface area and mesoporous structure of $Li_{0.4}CaTi_2O_4(OH)_2$ sample (Fig. 4) promote the

contact between electrode and electrolyte. According, the electrochemical properties improved with increasing x and reaches an optimum (in the present work, x=0.4), then decreases with further increasing x ((≥ 0.6) because of the appearance of $Li_{1.8}H_{0.19}Ti_2O$.

In summary, $CaTi_2O_4(OH)_2$ nanosheets exhibit good charge/discharge capacity. The charge/discharge capacity of $CaTi_2O_4(OH)_2$ nanosheets are significantly improved by doping Lithium. However, the cycling capability is poor (Fig. 6). It is suggested that the positive and negative charges balance plays a key role in electrochemical performance of the material. The effort to improve the capacity retention is ongoing.

4. CONCLUSIONS

A novel nanosheet-like morphology $Li_xCaTi_2O_4(OH)_2$ (x= 0, 0.05, 0.2, 0.4, 0.6 and 0.8) was prepared by a simple hydrothermal route. In comparison to pristine $CaTi_2O_4(OH)_2$ (initial irreversible loss of 33.2% and reversible capacity of 67 % from 5 to 40 th), $Li_{0.4}CaTi_2O_4(OH)_2$ material has demonstrated superior electrochemical performance (e.g. lower initial irreversible loss of 11.2% and higher reversible capacity of 86%). The improvement of $Li_{0.4}CaTi_2O_4(OH)_2$ sample could be ascribed to the slightly increased lattice constant, large specific surface areas and decreased particle size.

ACKNOWLEDGEMENT
The present work was supported by the National Natural Science Foundation (Grant No. 51172201), and Zhejiang Province Key Science & Technology Innovation Team, New Battery material and Application Science &Technology Innovation Team supports (2010R50013).

References

1. B. Sels, D. De Vos, M. Buntinx, F. Pierard, A. Kirsch-De Mesmaeker and P. Jacobs, *Nature*, 400 (1999) 855
2. V. R. Choudhary, D. K.Dumbre, B. S. Uphade, V. S. Narkhede, *J. Mol. Catal. A: Chem.*, 215 (2004) 129
3. L. Ren, J. He, S. Zhang, D. G. Evans, X. Duan, *J. Mol. Catal. B: Enzym.*, 18 (2002) 3
4. Aamir I. Khan and Dermot O'Hare, J. Mater. Chem., 12 (2002)3191-3198
5. L. Desigaux, M. B. Belkacem, P. Richard, J. Cellier, P. Léone, L. Cario, F. Leroux, C. Taviot-Guého and B. Pitard, *Nano. Lett.*, *6* (2006) 199-204
6. J. P. Liu, Y. Y. Li, X.T. Huang, G. Y. Li, and Z. K. Li, *Adv. Funct. Mater.* 18 (2008) 1448-1458
7. K.H. Goh, T.T. Lim , Z. L. Dong, *Water Res.*, 42 (2008) 1343-1368
8. M. P. A gnieszka, V. G. Cathie and E. Frackowiak, *Energ. Fuel.*, *24 (*2010**)** 3346-3351
9. L. B. Kong, J. W. Lang, M. Liu, Y. C. Luo, L. Kang, *J. Power Sources*, 194 (2009) 1194-1201
10. B.D. Cullity, Elements of X-Ray Diffraction, 2nd ed., Addison-Wesley, London, 1978
11. G. M. Sheldrick, *Acta Crys. A*, 46 (1990) 467
12. Z. Yuan, L. Wang, J. Wang, S. Xia, P. Chen, Z. Hou and X. Zheng, *Applied Catalysis B: Enviromental*, 101 (2011) 431-440
13. F. M. Labajos, M. D. Sastre, R. Trujillano and V. Rives, *J. Mater. Chem.*, 9 (1999) 1033-1039
14. T. Allen, Particle Size Measurement, 5th ed., Chapman and Hall: London, 1997

15. J. Y. Baek, H. Ha, I. Kim and S. Hwang, *J. Phys. Chem. C*, 113 (2009) 17392-17398
16. J. M. Tarascon and M. Armand, *Nature*, 414 (2001) 359-367
17. S. Wu, M. Chen, C. Chien and Y. Fu, *J. Power Sources*, 189 (2009) 440-444